Monthly Notices
of the
ROYAL ASTRONOMICAL SOCIETY

MNRAS **503,** 3297–3308 (2021)
Advance Access publication 2021 February 22

doi:10.1093/mnras/stab503

Chondrules from high-velocity collisions: thermal histories and the agglomeration problem

Nick Choksi [1]★ Eugene Chiang [1,2] Harold C. Connolly, Jr.,[3] Zack Gainsforth[4] and Andrew J. Westphal[4]

[1]*Astronomy Department, Theoretical Astrophysics Center, and Center for Integrative Planetary Science, University of California, Berkeley, CA 94720, USA*
[2]*Department of Earth and Planetary Science, University of California, Berkeley, CA 94720, USA*
[3]*Department of Geology, School of Earth and Environment, Rowan University, Glassboro, NJ 08028, USA*
[4]*Space Sciences Laboratory, University of California, Berkeley, CA 94720, USA*

Accepted 2021 February 17. Received 2021 February 16; in original form 2020 September 21

ABSTRACT

We assess whether chondrules, once-molten mm-sized spheres filling the oldest meteorites, could have formed from super-km s^{-1} collisions between planetesimals in the solar nebula. High-velocity collisions release hot and dense clouds of silicate vapour which entrain and heat chondrule precursors. Thermal histories of CB chondrules are reproduced for colliding bodies ∼10–100 km in radius. The slower cooling rates of non-CB, porphyritic chondrules point to colliders with radii $\gtrsim$ 500 km. How chondrules, collisionally dispersed into the nebula, agglomerated into meteorite parent bodies remains a mystery. The same orbital eccentricities and inclinations that enable energetic collisions prevent planetesimals from re-accreting chondrules efficiently and without damage; thus the sedimentary laminations of the CB/CH chondrite Isheyevo are hard to explain by direct fallback of collisional ejecta. At the same time, planetesimal surfaces may be littered with the shattered remains of chondrules. The micron-sized igneous particles recovered from comet 81P/Wild-2 may have originated from *in-situ* collisions and subsequent accretion in the proto-Kuiper belt, obviating the need to transport igneous solids across the nebula. Asteroid sample returns from *Hayabusa2* and *OSIRIS-REx* may similarly contain chondrule fragments.

Key words: comets: general – Kuiper belt: general – meteorites, meteors, meteoroids – minor planets, asteroids: general – planets and satellites: formation – protoplanetary discs.

1 INTRODUCTION

Beneath the fusion crusts of the most primitive stony meteorites lies a profusion of millimetre-sized igneous spheres. These chondrules, which can fill $\gtrsim$50 per cent of meteorite volumes, are among the oldest creations of the Solar system, with lead isotopic ages of 4.562–4.567 billion yr, and near-solar compositions in refractory elements. Petrologic studies indicate that chondrules were heated to melting temperatures for a few minutes, and cooled over hours to days. Their roundness implies that chondrules were melted while suspended in space, so that surface tension pulled their shapes into spheres. For reviews, see Connolly & Jones (2016) and Russell, Connolly & Krot (2018).

From the petrologic data, we can infer some rough orders of magnitude characterizing the chondrule formation environment. The fact that chondrules were at least partially molten implies an ambient temperature of $T \sim 2000$ K. A single chondrule radiating into vacuum at this temperature would cool off unacceptably fast, within seconds; therefore chondrules must have been immersed in, and kept warm by, a gas of high heat capacity, or a radiation bath maintained by an optically thick medium, or both. The former possibility is further supported by the retention of volatile elements – principally sodium – within some chondrules, requiring ambient Na partial pressures of the order of $\sim 10^{-3}$ bars while $T \sim 2000$ K (Alexander et al. 2008; Fedkin & Grossman 2013). Gas at 2000 K has a sound speed ranging from $c_s \sim 0.7$ to 3 km s^{-1}, depending on whether it is composed predominantly of silicates or hydrogen. A characteristic length scale for the formation environment is given by the sound speed multiplied by the cooling time, $R \sim 4 \times 10^4 \, \mathrm{km} \, (c_s/\mathrm{km\,s^{-1}})(t_{\mathrm{cool}}/10\,\mathrm{h})$.

These scales, which describe a formation setting that was hot, pressurized, and compact, do not recall those of the solar nebula (a.k.a. the protoplanetary disc), which for the most part was cold ($\lesssim$300 K), rarefied ($\lesssim 10^{-4}$ bar in hydrogen, and orders of magnitude less in other elements), and extensive (with disc scale heights $\gtrsim 10^7$ km; e.g. Armitage 2011; Williams & Cieza 2011). This mismatch argues against purely nebular processes for creating chondrules (e.g. Desch & Connolly 2002). Furthermore, the hydrogen-rich composition of the nebula does not provide the high oxygen fugacities (oxygen partial pressures) required to form the iron-rich silicates present in chondrules (e.g. Ebel & Grossman 2000; Grossman et al. 2008).

The comparatively small, fast, and energetic scales inferred from chondrule petrology may instead be compatible with collisions between planetesimals. Bodies on heliocentric orbits with eccentricities e and mutual inclinations i collide with relative velocities $u_{\mathrm{rel}} \sim \sqrt{e^2 + i^2} u_{\mathrm{K}}$, where u_{K} is the Keplerian orbital velocity ($u_{\mathrm{K}} \sim 20$ km s^{-1} in the main asteroid belt at 3 au).

★ E-mail: nchoksi@berkeley.edu

Impacts at $u_{\rm rel} \sim \mathcal{O}(1\,{\rm km\,s^{-1}})$ heat rock to a temperature of $T \sim \mu m_{\rm p} u_{\rm rel}^2/k \sim \mathcal{O}(10^3\,{\rm K})$, where $\mu \sim 30$ is the mean molecular weight of silicate gas, $m_{\rm p}$ is the proton mass, and k is Boltzmann's constant. The durations of heating and cooling should scale with the sizes of the colliding planetesimals. For example, if the colliding bodies are $R_{\rm pl} \sim \mathcal{O}(100\,{\rm km})$ in size, we might expect the initial fireball to last the 'smash-through' time of $R_{\rm pl}/u_{\rm rel} \sim \mathcal{O}(10^2\,{\rm s})$, consistent with a minutes-long heating event. The collisional destruction of the bodies releases an expanding cloud of debris and vapour, the thermodynamics of which could conceivably reproduce chondrule cooling rates. Fleshing out this possibility with a quantitative model is a goal of this paper.

Petrologic support for a collisional origin has been building, especially for CB/CH chondrites, whose metal nodules (a.k.a. blebs), lack of fine-grained matrix, and skeletal, non-porphyritic chondrule textures have been interpreted as signatures of melt production and vapour condensation from a hypervelocity impact, i.e. one fast enough to shock compress solids and produce melt and vapour (e.g. Campbell, Humayun & Weisberg 2002; Krot, Ivanova & Ulyanov 2007; Ivanova et al. 2008). Krot et al. (2005) found that CB chondrules crystallized 4–5 Myr after the formation of the oldest objects in the Solar system (calcium-aluminium-rich inclusions in CV chondrites) and argued that by this time, the solar nebula may have largely dissipated, ruling out a purely nebular origin. Fedkin et al. (2015) reproduced the elemental profiles of metal grains and chondrules in CB chondrites by modelling the condensation of an impact plume from a differentiated, water-rich asteroid.

Asphaug, Jutzi & Movshovitz (2011) pioneered numerical simulations of chondrule formation in planetesimal collisions, considering impact speeds $u_{\rm rel} \sim \mathcal{O}(100\,{\rm m\,s^{-1}})$, comparable to the surface escape velocities of $R_{\rm pl} \sim 100$ km asteroids. Collisions at these relatively low velocities do not melt solids; chondrules were instead envisioned to be liquid droplets sprayed out from planetesimal interiors made molten by ^{26}Al. Sanders & Scott (2012) argued that this scenario could resolve many of the petrologic difficulties of non-collisional formation models. Taking Asphaug et al. (2011) as a starting point, Hewins et al. (2018) numerically simulated the hydrodynamic and thermal evolution of a melt ejecta plume, finding thermal histories of plume gas parcels in good agreement with CB chondrule thermal histories determined experimentally.

A serious and still unsolved problem with colliding planetesimals with molten interiors is that such bodies are prone to chemically differentiate and produce droplets with non-solar compositions (Lichtenberg et al. 2018). Johnson et al. (2015) circumvented this difficulty by using higher velocity impacts to melt solar-composition solids directly; they found that at $u_{\rm rel} \gtrsim 2.5\,{\rm km\,s^{-1}}$, melt is created and jetted out of the impact site. Droplet sizes were estimated to be of the order of 1–10 mm for impactor diameters of 100–1000 km (see also Johnson & Melosh 2014). For these same parameters, chondrule cooling rates of 100–3000 K h^{-1}, compatible with experimental petrologic constraints, were inferred from radiative transfer modelling of the optically thick ejecta. In the impact simulations of Johnson et al. (2015) and Wakita et al. (2017, 2021), only a small fraction of the initially solid colliding mass, up to 7 percent, is jetted out as melt. Whether this efficiency of melt production is adequate to re-process enough of the main asteroid belt into the chondrites sampled on Earth is unclear.

Here we further explore a collisional genesis for chondrules. New developments in modelling shocked forsterite and silica demonstrate that vapour can be produced in abundance through hypervelocity impacts between planetesimals which are initially solid, at least in their outer layers (Kraus et al. 2012; Carter & Stewart 2020; Davies et al. 2020). Stewart et al. (2019b) suggested that the resulting hot silicate vapour cloud (a.k.a vapour plume) may be conducive to chondrule formation. We investigate this possibility by studying the hydrodynamic and thermodynamic evolution of the cloud, including its interaction with the hydrogen of the solar nebula. By contrast to Johnson et al. (2015) and related studies, we do not rely on melt created at the impact site to form chondrules. Actually, we do not model the impact dynamics at all. Instead we begin our analysis post-impact, assuming that a cloud of hot vapour has been released from the collision, and that this vapour contains initially solid or liquid debris. We study the subsequent evolution of this debris, including how it is heated and cooled by ambient vapour and radiation.

Our treatment of the vapour cloud and of the condensed particles embedded within it is zero-dimensional: we do not spatially resolve the cloud, but restrict our attention to its mean properties, e.g. density and temperature, and their evolution with time. Our model is similar in quantitative detail and complementary in scope to that of Dullemond, Stammler & Johansen (2014) and Dullemond et al. (2016); whereas they considered the evolution of a cloud containing essentially only molten chondrules, and no vapour except what outgasses from the melt, we study the converse problem of a pure vapour cloud in which solid/liquid particles are sparsely embedded. While the order-of-magnitude style of our approach precludes us from examining the complicated dynamics of the collision itself (cf. Johnson et al. 2015; Wakita et al. 2017, 2021; Davies et al. 2020), it does allow us to describe, broadly and intuitively, the simpler post-collision evolution of the silicate cloud, and to economically survey a range of possible outcomes. Our semi-analytic approach thus complements that of Stewart et al. (2019a), who presented an ab initio 3D smoothed particle hydrodynamics (SPH) numerical simulation of one vapourizing collision, and of Hewins et al. (2018), whose 3D adaptive-mesh simulation of a melt ejecta plume was initialized using the SPH impact model of Asphaug et al. (2011). While our fiducial parameters will be for the main asteroid belt, we will also scale our results to the proto-Kuiper belt, to see if we might also reproduce the chondrule-like thermal histories inferred from cometary samples returned by the *Stardust* mission (Nakamura et al. 2008; Jacob et al. 2009; Bridges et al. 2012; Gainsforth et al. 2015).

Just as important as the heating and cooling processes is the mechanism by which chondrules agglomerated into meteorite parent bodies. However they were melted, chondrules seem to have assembled into larger bodies with remarkable efficiency, as chondrites make up ~80 per cent of meteorite falls (Russell et al. 2018),[1] and chondrules fill the majority of chondrite volumes (Weisberg, McCoy & Krot 2006). Agglomeration must have occurred at velocities low enough to avoid shattering chondrules, no more so than in the CB/CH chondrite Isheyevo whose laminations point to gentle, sedimentary layering of size-sorted material (Garvie, Knauth & Morris 2017). Some have suggested that chondrules agglomerate immediately after a planetesimal collision, either re-accreting as fallout over days to weeks (Asphaug et al. 2011; Morris, Garvie & Knauth 2015), or collecting in local, potentially self-gravitating overdensities (Carter et al. 2019). Others posit that chondrules are dispersed into the solar nebula and gradually accreted on to planetesimals over the disc lifetime (Johansen et al. 2015; Hasegawa et al. 2016a, b). We will address the question of agglomeration in the context of high-velocity collisions between planetesimals.

[1]Modulo the bias of meteorite collections toward objects with sufficient material strength to survive the fall.

The rest of this paper is organized as follows. In Section 2, we describe our model of chondrule heating and cooling using a fiducial set of initial parameters appropriate to a vapourizing collision in the main asteroid belt of the solar nebula. There we also explore how our results vary over the space of initial cloud properties (density, temperature, size) and protoplanetary disc conditions, including those that might have characterized the proto-Kuiper belt. Section 3 tests several hypotheses for how chondrules might have agglomerated after their creation from high-speed collisions. A summary and outlook are given in Section 4.

2 VAPOUR CLOUD AND CHONDRULE THERMODYNAMICS

At a heliocentric distance of ∼3 au where the main asteroid belt resides, collisions fast enough to vapourize rock, with $u_{\rm rel} \gtrsim 3\,{\rm km\,s^{-1}}$, implicate crossing orbits having eccentricities and inclinations e, $i \gtrsim 0.1$. We stage our calculations at a time during the asteroid belt's past when the required ellipticities and inclinations have developed as a result of gravitational scatterings off large bodies (e.g. Carter & Stewart 2020; Raymond & Nesvorny 2020). During this era, dynamical heating competes effectively against drag exerted by residual nebular gas to keep at least the largest asteroids stirred. Thus we consider the collision of two planetesimals moving on elliptical and/or inclined orbits, and further assume the bodies to have roughly equal masses for simplicity.

Given our set-up, collisional debris, including silicate vapour, is ejected on to orbits having eccentricities and inclinations initially similar to those of their progenitors. This is in contrast to ambient nebular hydrogen which presumably traces circular heliocentric orbits. Thus the debris cloud will be moving relative to the surrounding hydrogen, at a speed equal to the cloud's non-circular heliocentric velocity. We adopt a fiducial speed for this 'nebular headwind' of $u_{\rm hw} = 3\,{\rm km\,s^{-1}}$ (equivalently $\sqrt{e^2+i^2} \simeq 0.15$). The nebular headwind will distort the initially overpressured and expanding vapour cloud into a shape resembling a cometary coma in the solar wind. Our calculations below will be restricted to the debris expanding directly into the headwind (the 'head' of the 'comet').

The debris cloud is assumed to be dominated by vapour and to contain in lesser proportions solid ejecta of various sizes, among which are chondrule precursors. The vapour is assumed to be sufficiently decompressed that it behaves as an ideal gas; we do not model the prior non-ideal phase of the explosion (cf. Johnson et al. 2015; Stewart et al. 2019a; Davies et al. 2020). Our fiducial input parameter values include the vapour cloud's initial radius, temperature, and mass density $(R_0,\ T_0,\ \rho_0) = (200\,{\rm km},\ 4000\,{\rm K},\ 10^{-5}\,{\rm g\,cm^{-3}})$; alternate parameters are explored in Section 2.4.2. Our analysis is restricted to zeroth-order properties of the cloud, e.g. its mean temperature and pressure. It may be that our assumption of a vapor-dominated plume is unrealistic; for a melt-dominated plume, see Dullemond et al. (2014).

We take the local density of the background hydrogen nebula to be $\rho_{\rm neb} = 10^{-11}\,{\rm g\,cm^{-3}}$, a factor of ten lower than that of the minimum-mass solar nebula at 3 au, and reflecting perhaps a more evolved disc. For a local nebular temperature of $T_{\rm neb} = 75\,{\rm K}$ (unheated by planetesimal bow shocks) and a mean molecular weight of $\mu_{\rm neb} = 2.4$ for solar composition gas, the nebular sound speed is $c_{\rm neb} = 0.5\,{\rm km\,s^{-1}}$.

Sections 2.1–2.3 describe, in chronological order, the dynamical and thermal evolution of the vapour cloud. Section 2.4 considers the evolution of a proto-chondrule, treated as a kind of test particle in the cloud.

2.1 Overpressured expansion and adiabatic cooling

At the start of our calculation (time $t = 0$), the cloud pressure greatly exceeds the nebular pressure, and the nebular mass displaced by the cloud is small compared to the cloud mass; thus the cloud expands nearly freely. We assume the expansion velocity u at this time is at its peak value, $u = \max u = u_0$, and is such that the cloud's bulk kinetic energy per unit mass, $(1/2)u_0^2$, is comparable to its internal energy $kT_0/[(\gamma-1)\mu m_{\rm p}]$ (Zel'dovich & Raizer 1967):

$$u_0 \sim \left(\frac{2kT_0}{(\gamma-1)\mu m_{\rm p}}\right)^{1/2} \sim 2.6\,{\rm km\,s^{-1}}\left(\frac{T_0}{4000\ {\rm K}}\right)^{1/2}, \quad (1)$$

where k is Boltzmann's constant, $m_{\rm p}$ is the proton mass, and $\mu = 30$ and $\gamma = 4/3$ (Melosh 1989) are the mean molecular weight and adiabatic index, respectively, of hot silicate vapour (see e.g. fig. 4 of Fegley & Schaefer 2012). The vapour mostly comprises Na and O atoms, and SiO and O_2 molecules whose ro-vibrational degrees of freedom are excited. In reality u_0 may be somewhat higher than given by (1) because the expansion speed at $t = 0$ respects how much thermal energy is present during the cloud's inception at $t < 0$, when the temperature may exceed T_0. We neglect this order-unity correction, which is also complicated by non-ideal-gas effects.

The cloud's initial expansion is supersonic with respect to the surrounding nebula, $u_0/c_{\rm neb} = 5$. A forward shock propagates outward, sweeping nebular hydrogen into a shell whose mass grows at a rate

$$\frac{{\rm d}M_{\rm neb}}{{\rm d}t} = 4\pi R^2(t)\rho_{\rm neb}[u(t)+u_{\rm hw}], \quad (2)$$

where $R(t)$ is the cloud's radius and $u(t) = \dot{R}$. In writing (2) we are considering the cloud's expansion directly against the headwind (so $u(t)$ and $u_{\rm hw}$ add), and idealizing the flow as spherically symmetric. The nebular gas carries an opposing momentum density $\rho_{\rm neb}u_{\rm hw}$ and forces the cloud to decelerate according to

$$\frac{\rm d}{{\rm d}t}\{[M_{\rm neb}(t)+M_0]\,u(t)\} = -4\pi R^2\rho_{\rm neb}u_{\rm hw}[u(t)+u_{\rm hw}], \quad (3)$$

where $M_0 = (4\pi/3)R_0^3\rho_0$ is the conserved mass of silicate material in the cloud. We numerically integrate equations (2) and (3) for $R(t)$, from which the mean density of silicates

$$\rho(t) = \rho_0\left(\frac{R}{R_0}\right)^{-3} \quad (4)$$

follows.

Initially, as the cloud expands, its mean temperature and pressure drop adiabatically from their starting values T_0 and $P_0 = \rho_0 kT_0/(\mu m_{\rm p})$:

$$\frac{T}{T_0} = \left(\frac{\rho}{\rho_0}\right)^{\gamma-1} \quad (5)$$

$$\frac{P}{P_0} = \left(\frac{\rho}{\rho_0}\right)^{\gamma} \quad (6)$$

with $\gamma = 4/3$ as stated earlier. These relations describe the silicate cloud material, not the piled-up nebular mass. When the vapour cools enough to condense, T and P deviate from these power-law adiabats, as will be described in Section 2.2.

In Fig. 1, panel (a) shows $R(t)$ (dashed black curve) and $\rho(t)$ (solid black curve), panel (b) shows $T(t)$ (solid blue curve), and panel (d)

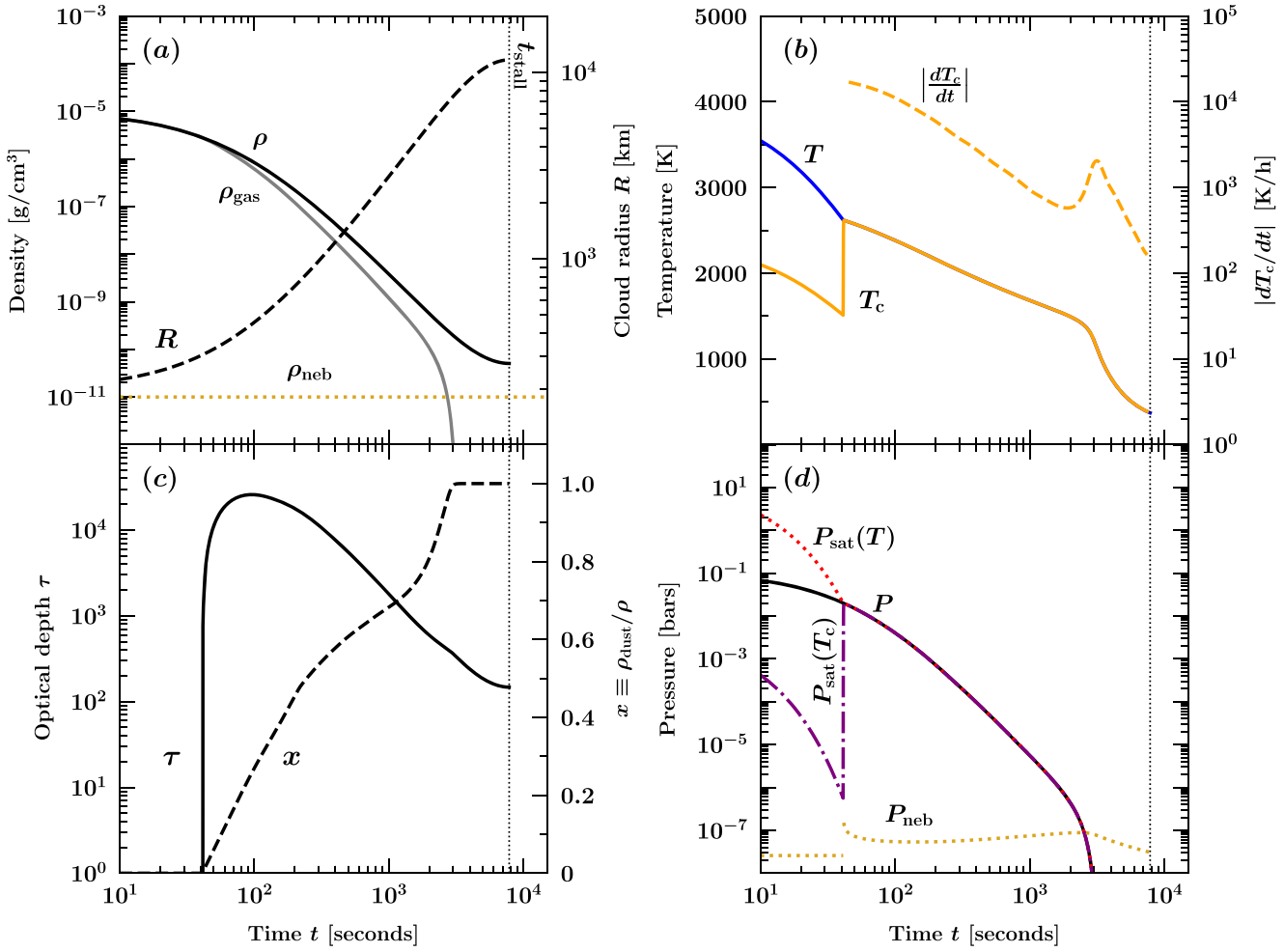

Figure 1. Evolution of the silicate vapour cloud and an embedded chondrule precursor of radius $s_c = 0.3$ mm. The cloud expands freely at first ($R \propto t$) and its total density ρ scales as $1/R^3$ (panel a). The cloud temperature T and pressure P initially fall adiabatically (panels b and d), while the proto-chondrule is heated conductively by the silicate vapour and cools by blackbody emission to reach an equilibrium temperature $T_c < T$ (panel b). The chondrule precursor does not vaporize because its saturation vapour pressure $P_{sat}(T_c) < P$ (panel d). At $t \sim 40$ s, the cloud saturates and vapour starts to condense into dust of mass fraction $x = \rho_{dust}/\rho$ (panel c); the gas density ρ_{gas} is now less than ρ (panel a). Once saturated, the cloud stays saturated with $P = P_{sat}(T)$, and for a time, T falls more slowly than along the original adiabat because of latent heat release. The nebular pressure P_{neb} just outside the cloud is higher than before dust condensation because of heating by dust-emitted radiation. The dust optical depth τ is always $\gg 1$ (panel c) but by $t \sim 3000$ s has decreased enough that radiative cooling causes T to drop faster, all of the remaining vapour to condense ($x = 1$), and P to nosedive. Radiative heating by dust enforces $T_c = T$; the chondrule cools along with the cloud over a couple hours (see also dT_c/dt in panel b). We end our calculation at $t_{stall} \sim 8000$ s ~ 2.2 h, when the nebular headwind has halted the cloud's expansion and ambient hydrogen starts to backfill the pressure-less cavity left by condensation.

shows $P(t)$ (solid black curve). For $t \lesssim 4 \times 10^3$ s, the cloud expands at near-constant velocity $u \simeq u_0$ so that $R \propto t$ and $\rho \propto t^{-3}$. Around $t \sim 4 \times 10^3$ s, the expansion slows from the swept-up nebular gas. We end our calculations when $u = 0$, at which point $t = t_{stall} \sim 8 \times 10^3$ s, $R = R_{stall} \sim 10^4$ km, and the silicate cloud density $\rho = \rho_{stall}$ is within a factor of 5 of ρ_{neb}. Section 2.3 discusses what happens after t_{stall}.

2.2 Condensation

The silicate vapour departs from the original adiabat at $t \sim 40$ s, when it cools sufficiently that it starts to re-condense into liquid/solid droplets (hereafter 'dust' – not to be confused with chondrules, which will not be discussed until Section 2.4). Condensation occurs when the saturation vapour pressure P_{sat} given by

$$\log_{10}\left(\frac{P_{sat}}{\text{bars}}\right) = -30.6757 - \frac{8228.146\ \text{K}}{T} + 9.3974 \log_{10}\left(\frac{T}{\text{K}}\right) \quad (7)$$

equals the cloud pressure P. We use here the vapour pressure for molten bulk silicate Earth ('BSE'), which has a chemical composition similar to that of olivine-rich chondrites (Fegley & Schaefer 2012). Once saturated, the cloud remains saturated, with the gas pressure P equal to $P_{sat}(T)$ (Zel'dovich & Raizer 1967; Melosh 1989).[2]

[2]The cloud may super-cool along the original adiabat before equilibrium condensation sets in. For our cloud whose expansion speed does not greatly exceed the thermal speed of its constituent gas molecules, and which may be full of impurities and condensation sites (i.e. liquid/solid ejecta from the original collision), this departure from equilibrium should be brief.

Condensation releases latent heat, which keeps the gas warmer than it would be along the original adiabat. The temperature of the dust–gas mixture evolves from adiabatic cooling, release of latent heat, and radiation emitted by dust:

$$\frac{4\pi\rho R^3}{3}\left(\left[C_{\rm gas}(1-x)+C_{\rm solid}x\right]{\rm d}T-\frac{k}{\mu m_{\rm p}}T\,(1-x)\,\frac{{\rm d}\rho}{\rho}\right.$$
$$\left.-\left[L_{\rm vap}-(C_{\rm solid}-C_{\rm gas})T\right]{\rm d}x\right)=-\frac{4\pi R^2\sigma_{\rm SB}T^4}{\tau}{\rm d}t. \quad (8)$$

The left-hand side of (8) is taken from Zel'dovich & Raizer (1967, chapter 8), where $x \equiv \rho_{\rm dust}/\rho$ is the mass fraction in condensates, $C_{\rm gas} = 6.3 \times 10^6$ erg/(g K) is the gas specific heat at constant volume (Melosh 1989), $C_{\rm solid} = 10^7$ erg/(g K) is the specific heat of dust, and $L_{\rm vap} = 3 \times 10^{10}$ erg g^{-1} is the heat of silicate vapourization (measured for pure forsterite; Nagahara, Kushiro & Mysen 1994). Whereas Zel'dovich & Raizer (1967) have no right-hand side term because they assume strict energy conservation, we account in our right-hand side for thermal photons that diffuse out of the assumed optically thick cloud, with $\sigma_{\rm SB}$ equal to the Stefan–Boltzmann constant and

$$\tau = \frac{3\rho R}{4\rho_{\rm solid}s_{\rm dust}}x \quad (9)$$

equal to the cloud radial optical depth, assuming that vapour condenses into dust grains of typical radius $s_{\rm dust}$ and internal density $\rho_{\rm solid} = 3$ g cm^{-3}. Each dust grain is assumed to present a geometric cross-section to photons. Our radiative loss term in (8) presumes that the cloud is in radiative equilibrium, with the bulk of the dust at temperature T heating photospheric dust near the cloud outer boundary to a temperature of $\sim T/\tau^{1/4}$. We take $s_{\rm dust} = 1$ μm, comparable in size to vapour condensates in other settings, including terrestrial experiments of condensing silicate and metal vapour (Melosh 1989, page 70), silicate clouds in exoplanet atmospheres (e.g. Gao et al. 2020), and vapour plumes of meteors impacting the Earth at $\lesssim$15 km s^{-1} (Johnson & Melosh 2012, their fig. 13). We test different values of $s_{\rm dust}$ in Section 2.4.2.

Equation (8) is solved numerically for $T(t)$ and $x(t)$, in conjunction with equations (2)–(4) for $R(t)$ and $\rho(t)$, and the condition $P = (1-x)\rho kT/(\mu m_{\rm p}) = P_{\rm sat}(T)$. Fig. 1 shows how, at $t \sim 40$ s, our fiducial cloud cools to $T \approx 2600$ K, at which point $P_{\rm sat}(T)$ crosses and subsequently locks to P (panel d). From here on out, dust condenses out of vapour and x grows from zero. Note the system temperature $T \approx 2600$ K at this time exceeds the value of $T \approx 1500$ K often taken to signal condensation. The latter is valid at low pressures, not the high pressures that characterize the impact plume. Our approach of comparing P to $P_{\rm sat}$ to decide when liquid droplets can condense out of vapour is more general than using a fixed temperature condition.

Over the next few minutes an order-unity fraction of the vapour condenses, rendering the cloud optically thick (panel c) and causing its temperature to drop more slowly with time than it did along the original adiabat because of latent heat release (panel b). We have verified that the cloud is in radiative equilibrium insofar as the photon diffusion time $\tau R/c$, where c is the speed of light, is either comparable to or less than the elapsed time t. We have also checked that gas and dust conduct heat to one another so efficiently (via gas–dust collisions) that both species are at very nearly the same temperature at any given time.

2.3 Radiative losses and nebular backfilling

Eventually, as the cloud expands and becomes less optically thick, an order-unity fraction of the cloud's thermal energy is lost to radiation. From Fig. 1(b), we see that radiative losses become significant at $t \sim 3000$ s. After this time, T declines faster than before, scaling somewhere between $T \propto s_{\rm dust}^{-1/3}t^{-5/3}$ and $T \propto s_{\rm dust}^{-1/3}t^{-1/3}$, as can be seen from equation (8) by ignoring the volume expansion and latent heat terms, taking a constant $x \sim 1$, and using either $R \propto t$ (free expansion) or $R \propto t^0$ (stalled expansion). The faster temperature decline causes residual silicate vapour to condense and the gas density to plummet (Fig. 1a).

Radiation losses and condensation thus cause the cloud's internal pressure to fall dramatically below the external nebular pressure (Fig. 1d). The cloud's momentum allows it to continue expanding against this adverse pressure gradient until $t_{\rm stall} \sim 8 \times 10^3$ s, when it comes to a stop and our calculation formally ends. After this point, we expect the headwind of nebular hydrogen to backfill the nearly pressure-free cavity, sweeping past whatever large fragments remain from the collision and carrying away chondrules and small condensates at speed $u_{\rm hw}$ (for more on this, see Section 3). Stewart et al. (2019a) miss this unidirectional headwind because their collision target was assumed unrealistically to be at rest relative to the nebular gas. The plume originating from their target thus undergoes a nearly spherical collapse, when it should be swept away by the headwind.

2.4 Chondrule thermal histories

Having described the evolution of the silicate cloud, we now examine how chondrules may be created within the cloud. We assume at $t = 0$ that the cloud, of size R_0, contains chondrule precursors, modelled as spheres of internal density $\rho_{\rm solid}$ and radius $s_{\rm c}$. These precursors were either condensed from the gas phase – as may have been the case for CB chondrules – or were ejected from the collision in solid or partially molten form and may thus contain relict grains.

It is not obvious that liquid/solid particles can survive without vapourizing if embedded in the cloud at $t < 0$, when $R < R_0$, $T > T_0$, and $\rho > \rho_0$. However, the collisional destruction of planetesimals is not instantaneous. It unfolds over the finite interval of time it takes the impactors to finish smashing through each other. For at least this initial smash-through phase, which lasts $\mathcal{O}(1$ min) for ~100 km-sized planetesimals, debris should be continuously generated and released into the vapour cloud. While debris that is released when the impactors first make contact may not last to $t = 0$, liquid/solid particles that are released towards the end of the smash-through phase, just before $t = 0$, may survive.

As we do not model the complicated dynamics of the collision (cf. Stewart et al. 2019b), we cannot determine how many chondrule precursors are created by gas-phase condensation or are ejected directly from the planetesimals and survive vapourization. We proceed by assuming that such particles exist and are entrained by the cloud, and that their combined mass is less than the cloud mass ($= 4\pi R_0^3\rho_0/3$), so that we may neglect how the particles affect the cloud's expansion. Order-of-magnitude estimates suggest these particles have chondrule-like sizes. A liquid droplet moving through vapour must be small enough that the surface tension force holding it together, $\sim 2\pi\sigma s_{\rm c}$, exceeds the disruptive force of aerodynamic drag, $\sim \rho_0 s_{\rm c}^2 u_0^2/2$ (Melosh 1989). For our fiducial parameters, this limiting size is $s_{\rm c} \sim 4\pi\sigma/(\rho_0 u_0^2) \sim \mathcal{O}(0.1$ mm), for a surface tension $\sigma \sim 350$ dyne cm^{-1} appropriate to molten rock. Using similar arguments, Melosh & Vickery (1991) and Johnson & Melosh (2014) found that molten ejecta are shredded into millimetre-scale droplets. Particles of this size are readily entrained in the vapour cloud; right at the outset of the cloud's expansion, the aerodynamic stopping times $t_{\rm stop} \sim \rho_{\rm solid}s_{\rm c}^3 u/F_{\rm drag}$ of mm-sized particles are orders

of magnitude shorter than the cloud dynamical time R/u, for a drag force $F_{\rm drag} \sim \rho u^2 s_{\rm c}^2$.

We now describe the thermal histories of these entrained particles.

2.4.1 *Chondrule thermal history, fiducial asteroid belt model*

Proto-chondrules exchange heat with their environment by gas conduction and radiation. Their temperature $T_{\rm c}$ evolves as

$$\frac{4\pi}{3} s_{\rm c}^3 \rho_{\rm solid} C_{\rm solid} \frac{dT_{\rm c}}{dt} = n_{\rm gas} \pi s_{\rm c}^2 u_{\rm th} k (T - T_{\rm c}) + 4\pi s_{\rm c}^2 \sigma_{\rm SB} \left(T^4 - T_{\rm c}^4\right), \quad (10)$$

where $n_{\rm gas} = (1-x)\rho/(\mu m_{\rm p})$ is the number density of gas molecules, $u_{\rm th} = \sqrt{8kT/(\pi \mu m_{\rm p})}$ is the gas mean thermal speed, and each collision between a gas molecule and a chondrule is assumed to transfer an energy $k(T - T_{\rm c})$. The heating term proportional to $\sigma_{\rm SB} T^4$ is due to the background radiation field emitted by optically thick dust (after it condenses). What equation (10) omits is drag-heating by the silicate vapour, but this effect lasts only briefly, for the fraction of a second it takes the chondrule to come up to speed with the cloud, and even then adds only marginally to conductive heating.

We set the proto-chondrule's initial temperature $T_{\rm c}(0) = 10^3$ K, a value within the wide range of temperatures to which solids are heated upon impact (depending principally on distance from the impact site; see fig. 2 of Johnson & Melosh 2014). This initial temperature is quickly forgotten as the proto-chondrule comes into thermal and dynamical equilibrium with the cloud. Equation (10) is solved for $T_{\rm c}(t)$ using a fiducial chondrule radius $s_{\rm c} = 0.3$ mm, with the background variables $n_{\rm gas}(t)$ and $T(t)$ calculated separately as described in previous sections.

Fig. 1(b) shows $T_{\rm c}(t)$. Initially, conductive heating is balanced by radiative cooling into the optically thin cloud (dust has not yet condensed), and the chondrule is at a temperature of $T_{\rm c} \sim 2000$ K. The saturation vapour pressure of the chondrule, $P_{\rm sat}(T_{\rm c})$ (equation 7), sits more than two orders of magnitude below the ambient gas pressure P (Fig. 1d), safeguarding the chondrule against vapourization (for a study of the time-dependent kinetics of vapourization and volatile retention, see Dullemond et al. 2016). Over the next ∼30 s, the chondrule remains colder than, but cools in lockstep with, the adiabatically expanding background gas, falling to $T_{\rm c} \sim 1500$ K. At $t \sim 40$ s, the chondrule heats back up to ∼2600 K when dust condenses and renders the entire cloud optically thick – the chondrule is literally 'flash-heated' by the radiation emitted by newly condensed dust (as discussed in Section 2.2, condensation is possible for T as high as 2600 K because the high cloud pressures cross the saturation vapour pressure). The chondrule is now trapped in this radiation bath and $T_{\rm c} \simeq T$. Over the course of ∼5 min, the temperature falls from ∼2600 K through the liquidus of ∼2000 K (below which melt and solid co-exist); it then passes through the solidus, here estimated to be ∼1500 K (below which the particle is entirely solid), after ∼30 min. Cooling rates $|{\rm d}T_{\rm c}/{\rm d}t|$ are plotted versus t in Fig. 1(b) and versus $T_{\rm c}$ in Fig. 2. Above the liquidus, $|{\rm d}T_{\rm c}/{\rm d}t| \sim 3000$–$20\,000$ K h^{-1}, while below the liquidus $|{\rm d}T_{\rm c}/{\rm d}t| \sim 300$–$3000$ K h^{-1}. These cooling rates appear compatible with empirically determined chondrule cooling rates (e.g. Desch & Connolly 2002; Connolly & Jones 2016), shown as grey regions in Fig. 2. They also overlap with the cooling rates determined empirically for CB chondrules by Hewins et al. (2018). Fig. 2 shows that adiabatic cooling alone predicts cooling rates that exceed sub-liquidus experimental rates by at least an order of magnitude; cooling buffered by dust condensation is essential to reproducing chondrule cooling rates.

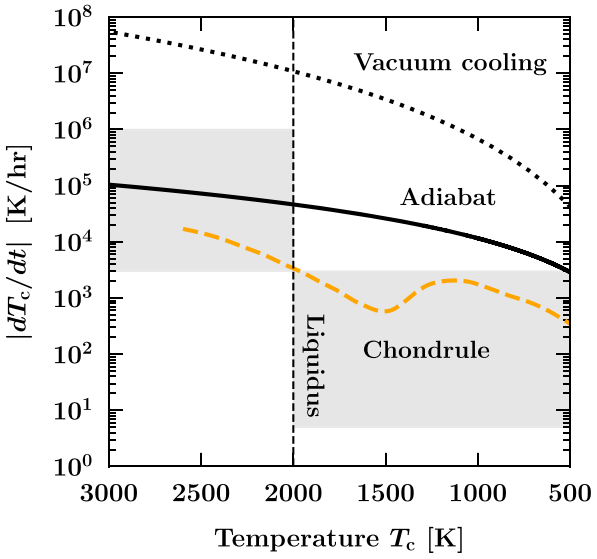

Figure 2. Chondrule cooling rate versus temperature (dashed orange curve), shown from the point the cloud saturates (in this regime radiation by newly condensed dust enforces $T_{\rm c} = T$, and $T_{\rm c}$ falls monotonically). From $T_{\rm c} = 2600$ K down to $T_{\rm c} = 1500$ K, cooling is mostly driven by the cloud's expansion, with cooling rates lower than given by the original adiabat (solid curve) which does not account for latent heat released by condensation. Also shown for comparison is the blackbody cooling rate in vacuum ($-{\rm d}T_{\rm c}/{\rm d}t = 4\pi s_{\rm c}^2 \sigma_{\rm SB} T_{\rm c}^4/(4\pi \rho_{\rm solid} s_{\rm c}^3 C_{\rm solid}/3)$; dotted curve). For $T_{\rm c} \lesssim 1500$ K, radiative losses from the cloud as a whole become important and the cooling rate increases. The shaded regions highlight super and sub-liquidus cooling rates inferred from laboratory experiments. These constraints are taken from Desch & Connolly (2002), except for the poorly constrained upper bound to the super-liquidus cooling rate which we arbitrarily set at 10^6 K h^{-1}.

2.4.2 *Cooling rate variations over parameter space*

We explore how chondrule cooling rates change with initial cloud properties ρ_0, R_0, and T_0, as well as the sizes of condensed dust grains $s_{\rm dust}$ and the background nebular density $\rho_{\rm neb}$. Unless otherwise indicated, we vary one parameter at a time while holding others fixed at their fiducial values $(\rho_0, R_0, T_0, \rho_{\rm neb}, s_{\rm dust}) = (10^{-5}\,{\rm g\,cm^{-3}}, 200\,{\rm km}, 4000\,{\rm K}, 10^{-11}\,{\rm g\,cm^{-3}}, 1\,\mu{\rm m})$.

Fig. 3 plots chondrule cooling rates starting from when vapour saturates, dust forms, and the chondrule temperature $T_{\rm c}$, radiatively locked to the cloud temperature T, falls monotonically (see Fig. 2). Fig. 3(a) varies the cloud's initial radius R_0 and initial density ρ_0, and demonstrates that what matters for the cooling rate ${\rm d}T_{\rm c}/{\rm d}t$ at a given temperature T is the product $\rho_0 R_0^3$, i.e. the total cloud mass $M_{\rm cloud} = 4\pi\rho_0 R_0^3/3$. This dependence follows from

$$\frac{{\rm d}T_{\rm c}}{{\rm d}t} = \frac{{\rm d}T}{{\rm d}t} = \frac{{\rm d}T}{{\rm d}\rho}\frac{{\rm d}\rho}{{\rm d}R}\frac{{\rm d}R}{{\rm d}t}. \quad (11)$$

The factor ${\rm d}T/{\rm d}\rho$ depends only the equilibrium thermodynamics of adiabatic cooling and condensation, which specifies $\rho(T)$ (equation 8); it does not depend on the initial conditions ρ_0 or R_0. The second factor ${\rm d}\rho/{\rm d}R \propto \rho/R$ (equation 4), which for given $\rho(T)$ scales as $1/R \propto M_{\rm cloud}^{-1/3}$. The final factor ${\rm d}R/{\rm d}t$ is nearly constant ($=u_0$) at early times when the cloud is freely expanding, and depends only on $\rho(T)$ and $u_{\rm hw}$ in the final stages of the expansion just before the cloud stalls. Putting it all together, we see that ${\rm d}T_{\rm c}/{\rm d}t$ scales as $M_{\rm cloud}^{-1/3}$ at all times; a more massive cloud cools more slowly because to reach a given $\rho(T)$ it needs to expand to a larger radius R, when its dynamical time $R/\dot{R}$ is longer.

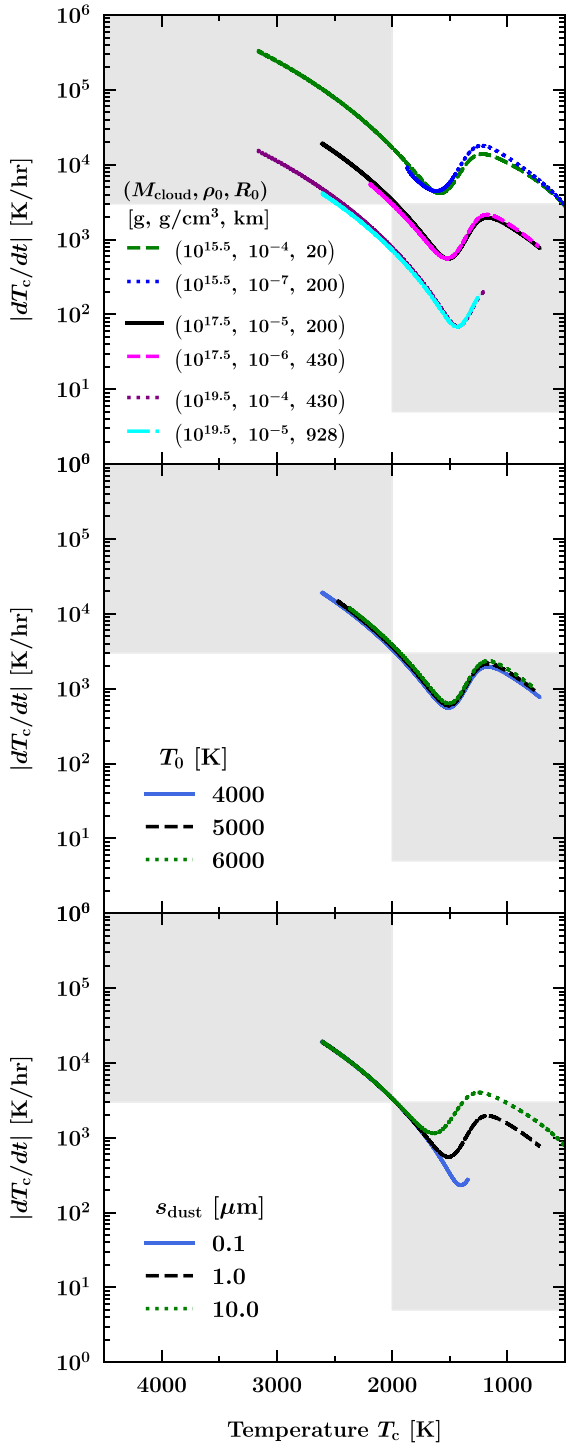

Figure 3. *Top*: Chondrule cooling rates versus temperature (as in Fig. 2) for various initial cloud densities ρ_0 and radii R_0. Cooling rates scale with the total cloud mass, $\mathrm{d}T_{\rm c}/\mathrm{d}t \propto M_{\rm cloud}^{-1/3}$ (equation 11), where $M_{\rm cloud} \sim \rho_0 R_0^3$. Cooling rates satisfy experimental constraints (shaded regions) for $M_{\rm cloud} \gtrsim 10^{17}$ g. *Middle*: Cooling rates for different initial cloud temperatures T_0. The value of T_0 has little effect on cooling rates because cooling is governed by the equilibrium condition $P = P_{\rm sat}(T)$ which is independent of initial conditions. *Bottom*: Cooling rates for different assumed radii $s_{\rm dust}$ of condensed dust grains. The dust size does not matter at higher temperatures (early times) when the cloud cools by expanding and loses negligible energy to radiation. Larger dust grains render the cloud less optically thick and hasten the onset of radiative losses, which increase cooling rates.

According to Fig. 3(a), cloud masses $M_{\rm cloud} \sim 10^{17}$–$10^{20}$ g yield chondrule sub-liquidus cooling rates consistent with the fastest rates inferred from petrologic experiments, in particular the ∼100–1000 K h^{-1} rates inferred for skeletal, non-porphyritic CB chondrules (Hewins et al. 2018). The impact cloud can only be less massive than the colliding asteroids from which it derives; $M_{\rm cloud} \sim 10^{17}$–$10^{20}$ g imposes hard lower limits on the combined radius of the colliding planetesimals of $R_{\rm pl} \gtrsim [3M_{\rm cloud}/(4\pi\rho_{\rm solid})]^{1/3} \sim 2$–20 km. If we assume a vapour production efficiency of 1 per cent by mass (cf. Johnson et al. 2015; Wakita et al. 2017, 2021; these studies technically track melt and not vapour), the colliding planetesimals would be 10–100 km in radius, similar in size to the asteroids that contain most of the main belt mass today, and perhaps also in the past (Morbidelli et al. 2009).

The value of T_0 does not much affect the cooling rate post-saturation (Fig. 3b), when $P = P_{\rm sat}(T)$ and the cloud thermodynamics evolves in an equilibrium fashion with initial conditions largely forgotten. What small differences can be seen in Fig. 3(b) for $\mathrm{d}T_{\rm c}/\mathrm{d}t$ arise from variations in the free-expansion cloud velocity $u_0 \propto T_0^{1/2}$ (equation 1).

Fig. 3(c) varies $s_{\rm dust}$, the assumed radii of dust grains that condense out of the silicate vapour. At the earliest times, when cooling is driven by expansion and not by radiation, $s_{\rm dust}$ is irrelevant. Radiation becomes important sooner, and cools the cloud faster, for larger $s_{\rm dust}$ which makes the cloud less optically thick (equation 9). The radiation-dominated cooling rate $\mathrm{d}T_{\rm c}/\mathrm{d}t = \mathrm{d}T/\mathrm{d}t$ at a given T (not t) scales between $s_{\rm dust}^{1/5}$ during free expansion and $s_{\rm dust}^{1}$ as the cloud stalls. This can be seen from equation (8) in combination with the scalings $T \propto s_{\rm dust}^{-1/3} t^{-5/3}$ and $T \propto s_{\rm dust}^{-1/3} t^{-1/3}$ as derived in Section 2.3, with t substituted in favour of T.

2.4.3 *Collisions in the proto-Kuiper belt*

The *Stardust* spacecraft discovered that the short-period comet 81P/Wild-2 contains chondrule-like particles (e.g. Nakamura et al. 2008). By 'chondrule-like' we mean igneous particles having mineralogies and textures, and by extension thermal histories, similar to those of asteroidal chondrules. The particles collected have sizes up to ∼ 10 μm. Sampling larger particles would have required the *Stardust* spacecraft to approach closer to the comet than was considered safe.

To assess whether high-velocity collisions can explain the heating experienced by these cometary particles, we re-scale our model to heliocentric distances possibly appropriate to Wild-2's formation. Short-period comets like Wild-2 originate as Kuiper belt objects (KBOs), predominantly of the 'scattered' variety having relatively large orbital eccentricities and inclinations (e.g. Nesvorný et al. 2017). Dynamically hot KBOs are thought to reflect a period of upheaval when the orbits of the giant planets (and perhaps those of planets no longer present) underwent large-scale changes driven by gravitational scatterings with remnant planetesimals (e.g. Fernandez & Ip 1984; Malhotra 1995; Gomes et al. 2005; Tsiganis et al. 2005; Ford & Chiang 2007; Levison et al. 2011; Dawson & Murray-Clay 2012). During this time, Neptune and proto-KBOs were propelled outwards from ∼10–20 to 30 au and beyond. Accordingly, we re-stage our calculations for $a = 15$ au, near where proto-KBOs may have originated. We adopt a nebular density $\rho_{\rm neb} = 1.1 \times 10^{-13}$ g cm^{-3}, a factor of 90 lower than our fiducial value at 3 au, as follows from the scaling law $\rho_{\rm neb} \propto a^{-39/14}$ derived for the solar nebula (e.g. Chiang & Youdin 2010). For simplicity we keep all other model parameters fixed at their fiducial values; this assumes the lower heliocentric velocity at 15 au versus 3 au is

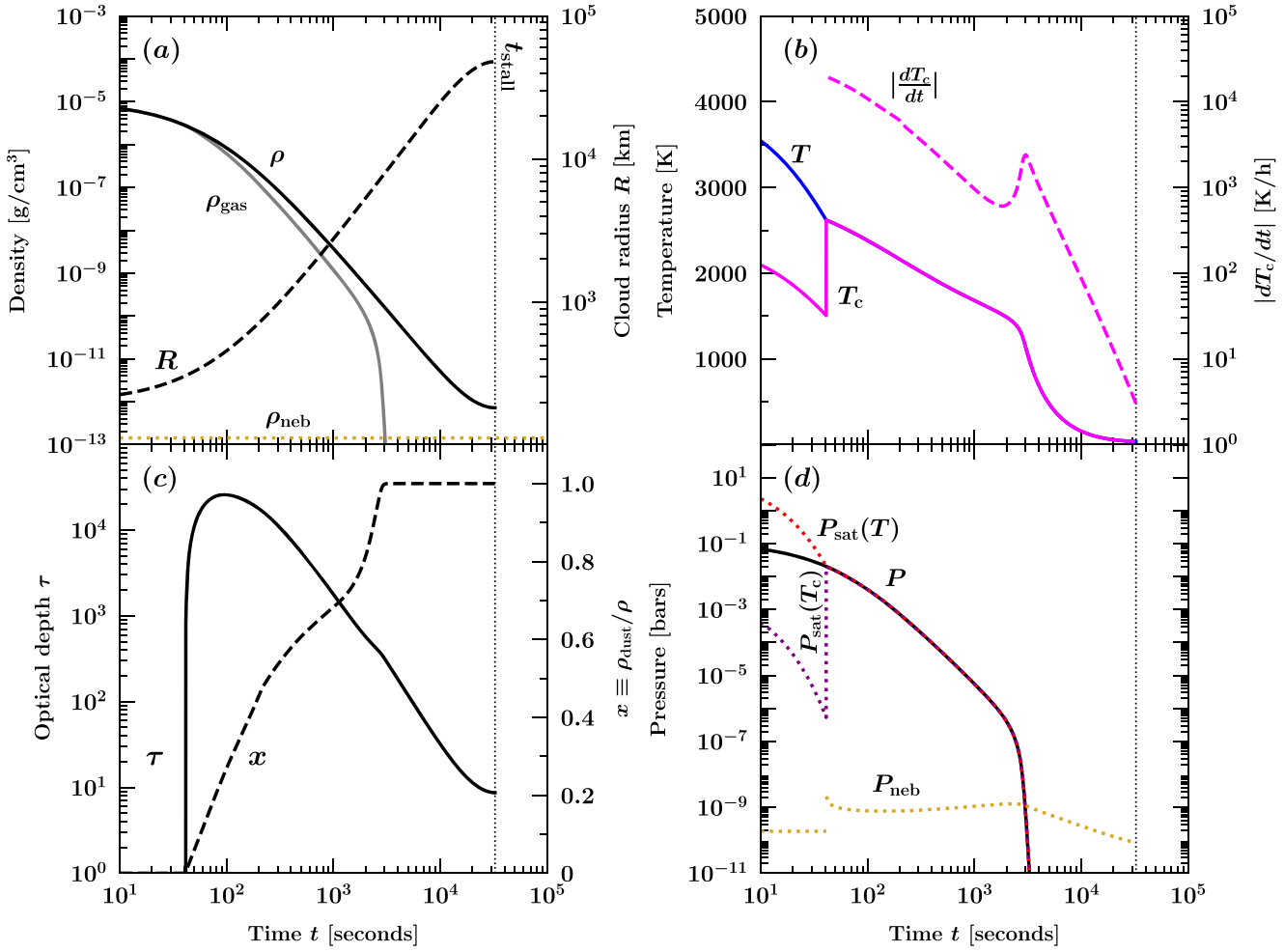

Figure 4. Same as Fig. 1, but for a vapour cloud created at $a = 15$ au in a nebula of density $\rho_{neb} = 1.1 \times 10^{-13}$ g cm^{-3}, conditions intended to model those of the proto-Kuiper belt where comet Wild-2 may have formed. The change in scenery does not much affect the thermal evolution of either the silicate cloud or the chondrule at temperatures $T \gtrsim 1000$ K and times $t \lesssim 5 \times 10^3$ s. The main difference in cloud evolution between asteroid belt and Kuiper belt distances is at late times. Because the nebular density ρ_{neb} is lower at 15 au than at 3 au, the nebula is less effective at slowing down the cloud, which does not stall until $t_{stall} = 3.5 \times 10^4$ s, a factor of 4 later than the stalling time at 3 au.

compensated by higher orbital eccentricities and/or inclinations, to keep the relative collision velocity between planetesimals, and by extension the nebular headwind velocity u_{hw}, unchanged. Note also that we keep our fiducial chondrule size at $s_c = 0.3$ mm, as this is still presumably the characteristic melt droplet size set by the balance between surface tension and ram pressure disruption by the expanding vapour (Section 2.4).

Comparison of Fig. 1 with Fig. 4 demonstrates what one might have expected: for a given set of initial cloud conditions (ρ_0, T_0, R_0), thermal histories of cloud-embedded particles at 15 au are qualitatively the same as at 3 au. The chondrule thermal evolution is controlled by the internal thermodynamics of the vapour cloud which are not especially sensitive to nebular environment, especially when the cloud is still hot and the chondrule is passing through the liquidus. This is further evidenced in Fig. 5. Sub-liquidus cooling rates dT_c/dt for a given T are marginally faster in the proto-Kuiper belt than in the asteroid belt because the lower nebular density at larger heliocentric distance allows the cloud to expand freely for longer.

While we have so far focused on generating chondrule-like thermal histories, comets like Wild-2 are replete with other kinds of equilibrated aggregates (EAs) which were also once partially molten, but which are smaller (0.1–1 μm), attained lower peak temperatures (∼1200 K), and skew towards faster cooling rates ($\gtrsim$500 K h^{-1}; Bradley 1994; Brownlee et al. 2005; Messenger, Keller & Nguyen 2013). In our model, cooling rates scale inversely with the cloud mass, $dT/dt \propto M_{cloud}^{-1/3}$, with $M_{cloud} \gtrsim 10^{17}$ g required to produce the cooling rates exhibited by chondrules (Section 2.4.2). Lower mass clouds, in the range $M_{cloud} \sim 10^{15}$–10^{17} g, might have hosted the faster cooling EAs; cloud masses and peak temperatures may have been systematically smaller in the proto-Kuiper belt where orbital velocities were slower, and collisions less violent, than in the asteroid belt.

3 AGGLOMERATION INTO METEORITE PARENT BODIES

In this section, we assess various avenues for agglomerating chondrules into larger bodies. We continue in the context of the aftermath of a high-speed collision between two roughly equal-mass plan-

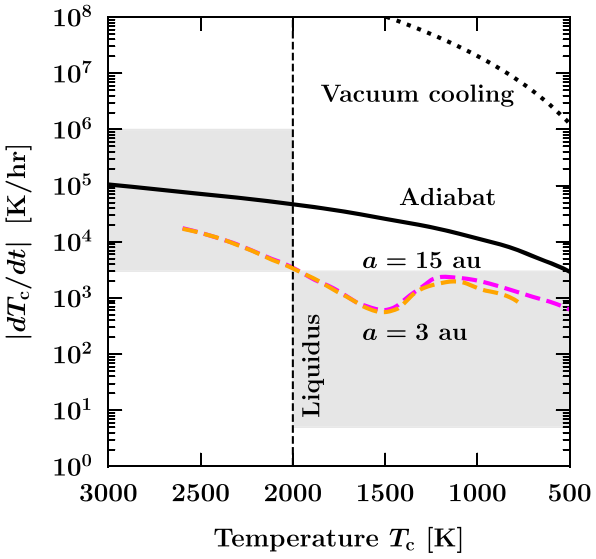

Figure 5. Comparison of chondrule cooling rates at 3 au in the asteroid belt (as in Fig. 2) and at 15 au in the proto-Kuiper belt. Collisional vapour clouds have thermal histories that are practically independent of heliocentric distance and might thus explain the thermal histories of chondrule-like particles discovered by *Stardust*. Cooling is somewhat faster at 15 au than at 3 au because at larger distances the cloud is less impeded by a less dense nebula, and so expands faster.

etesimals, though some of our ideas may apply to other chondrule formation scenarios.

We return to our fiducial asteroid belt model and begin our consideration of agglomeration at time $t_{\rm stall} = 8 \times 10^3$ s, when dust and chondrules are dispersed across a cloud of size $R_{\rm stall} \sim 10^4$ km. Because one or both of the planetesimals that originally collided to produce the cloud were moving on eccentric and inclined orbits, the debris cloud will initially trace an eccentric and inclined orbit as well. Accordingly the debris, including large post-collision fragments, will encounter a headwind of nebular hydrogen at speed $u_{\rm hw} \sim 3\,{\rm km\,s^{-1}}\,(\sqrt{e^2+i^2}/0.15)\,(3\,{\rm AU}/a)^{1/2}$, assuming that the nebular gas occupies circular orbits. Just after $t_{\rm stall}$, the headwind will flood the near pressure-less volume occupied by dust, chondrules, and post-collision fragments, filling it over a time-scale $R_{\rm stall}/u_{\rm hw} \sim 3 \times 10^3$ s – probably somewhat longer, since the inertia of the stalled debris cloud, whose mean density $\rho_{\rm stall}$ is ∼5 times higher than the nebular headwind density $\rho_{\rm neb}$, will slow the headwind by an order-unity factor.

Newborn chondrules become entrained in the supersonically streaming nebular headwind over a momentum stopping time

$$t_{\rm stop} \sim \frac{\rho_{\rm solid}}{\rho_{\rm neb}} \frac{s_{\rm c}}{u_{\rm hw}} \sim 3 \times 10^4\,{\rm s} \left(\frac{\rho_{\rm neb}}{10^{-11}\,{\rm g/cm^3}}\right)^{-1} \left(\frac{s_{\rm c}}{0.3\,{\rm mm}}\right) \left(\frac{u_{\rm hw}}{3\,{\rm km\,s}}^{-1}\right)^{-1}. \quad (12)$$

Over this aerodynamic drag time-scale, chondrules produced by the collision are swept into the background nebula and join its circular motion. Large post-collision fragments cannot circularize as quickly as chondrules and dust do, and will continue moving on eccentric orbits, at least initially.

3.1 Agglomeration on to existing planetesimals

We first ask whether newly formed chondrules can be re-accreted on to the post-collision remains of their progenitor asteroids. For concreteness, we consider a remnant solid body (possibly a collection of re-assembled fragments) of radius $R_{\rm pl} \sim 100$ km, typical of the asteroid and Kuiper belt today (Morbidelli et al. 2009; Sheppard & Trujillo 2010).

The remnant asteroid's cross-section for accreting chondrules is geometric and not enhanced by gravitational focusing. This is because relative velocities between the asteroid and nebula-entrained chondrules are of the order of $u_{\rm hw}$, which is likely greater than the asteroid surface escape velocity $u_{\rm esc} \sim 100\,{\rm m\,s^{-1}}$. In principle, gas drag can abet gravity to enlarge accretion cross-sections ('pebble accretion'; Ormel & Klahr 2010), but our standard $u_{\rm hw} \sim 3\,{\rm km\,s^{-1}}$ headwind sweeps chondrules past the body too quickly for gravity to be significant. One could entertain slower headwinds by colliding planetesimals moving on more circular, less inclined orbits; but for $u_{\rm hw}$ to be less than $u_{\rm esc} \sim 100\,{\rm m\,s^{-1}}$, eccentricities and inclinations would have to be $<5 \times 10^{-3}$, which runs counter to our premise of high-velocity collisions in a dynamically hot belt (Raymond & Izidoro 2017; Carter & Stewart 2020; Raymond & Nesvorny 2020).

Since gravitational focusing is defunct, of the chondrules dispersed from the collision over a scale $R_{\rm stall}$, only a tiny fraction

$$f_{\rm agglom} \sim \left(\frac{R_{\rm pl}}{R_{\rm stall}}\right)^2 \sim 10^{-4} \quad (13)$$

can be re-accreted, corresponding to those chondrules that happen to lie directly in the path of the remnant asteroid. Our value of $f_{\rm agglom}$ is orders of magnitude lower than the re-accretion efficiency of ∼0.03 estimated by Morris et al. (2015, their section 3.3). Their analysis, which assumes that chondrules are 'swept up' by the remnant asteroid at speeds ranging from 25 to 500 m s^{-1} (their sweep-up velocities are equivalent to our headwind velocities), overestimates gravitational focusing. Their factor by which the accretion cross-section is enhanced by gravity is evaluated using a 'random', presumably particle–particle velocity of 1 m s^{-1}, when it should use instead the particle-asteroid relative velocity, which is at least 25 m s^{-1} according to their model. Thus their estimate for the gravitational focusing factor is internally inconsistent; it is too large by a factor of at least $25^2 = 625$. Correcting for this implies the depth of their re-accreted particle layer is unacceptably thin, on the order of a millimetre, not a metre as claimed.

While we have shown that a given chondrule is unlikely to be re-accreted by the remains of its progenitor asteroids, it could, in principle, be accreted by another body elsewhere. Impact velocities would have to be low enough to avoid shattering the chondrule. Laboratory experiments find mm-sized particles fragment at impact speeds as low as ∼25 m s^{-1} (Wurm, Paraskov & Krauss 2005; Teiser & Wurm 2009).[3] Such relative speeds, which require e, $i \lesssim 10^{-3}$, might be achieved for planetesimal accretors small enough that the circularizing/flattening effects of nebular gas drag overwhelm gravitational stirring by larger bodies. These small-body accretors would be much smaller than the original colliding pair of eccentric/inclined planetesimals. Note that even if the small-body accretors have vanishing e, i, there is a floor on the chondrule-accretor relative velocity of $c_{\rm neb}^2/(2u_{\rm K}) \sim 10$ m s^{-1} which arises because disc

[3]Chondrule fragments are occasionally observed (e.g. Nelson & Rubin 2002) and chondrule rims and matrix may be shattered chondrules (Alexander, Hutchison & Barber 1989). But the fact remains that the overwhelming majority of chondrules are round and intact.

gas and its entrained chondrules rotate at sub-Keplerian speeds, while the accretors have Keplerian velocities (Weidenschilling 1977).

Shattering upon accretion may be a feature rather than a bug in the context of comet 81P/Wild-2, whose thermally processed, micron-sized particles have been described as 'chondrule and CAI-like fragments' (Brownlee, Joswiak & Matrajt 2012). Perhaps mm-sized melt droplets strewn across the outer Solar system by planetesimal collisions were broken up into micron-sized fragments upon being accreted by comet progenitors/Kuiper belt objects. Low efficiencies of accretion might not be a problem either, in so far as micro-chondrules make up only a small fraction of the volume of the comet.

3.2 Self-gravity

Can chondrules produced from a collision collapse under their own self-gravity? A necessary but not sufficient condition for gravitational collapse is that the local density exceed

$$\rho_{\rm Roche} \approx \frac{3.5 M_\odot}{a^3} \approx 8 \times 10^{-8}\,{\rm g\,cm^{-3}} \left(\frac{a}{3\,{\rm au}}\right)^{-3}, \quad (14)$$

the minimum density a self-gravitating body must have to resist tidal disruption by the central star (e.g. Chiang & Youdin 2010). For our fiducial parameters, the mean density of the cloud of dust and chondrules just after it re-fills with nebular gas is $\rho_{\rm stall} + \rho_{\rm neb} \sim 6\rho_{\rm neb}$, which falls short of $\rho_{\rm Roche}$ by three orders of magnitude. Thus the cloud as a whole will eventually be sheared apart by solar tides and phase-mixed with the rest of the nebula over a time-scale of order the orbital period, $\sim 10^8$ s at 3 au.

Might there be localized overdensities of particles that self-gravitate? In their hydrodynamic simulation of a collision between ~100-km sized asteroids, Carter et al. (2019) found clumps of debris having densities exceeding $\rho_{\rm Roche}$ and suggested they might collapse to form ~10-km sized planetesimals. These overdensities may be spurious if they arise from the unrealistic near-spherical collapse of their vapor plume (see end of section 2.3). Regardless, for a clump to self-gravitate it is not sufficient to satisfy the Roche criterion against tidal disruption; the Jeans criterion comparing self-gravity to gas pressure must also be met. For a clump having particle density $\rho_{\rm particle}$ and gas density $\rho_{\rm gas}$ to be bound, it must be at least as large as the Jeans length

$$R_{\rm Jeans} \sim \frac{c_{\rm neb}(1+\rho_{\rm particle}/\rho_{\rm gas})^{-1/2}}{\sqrt{G(\rho_{\rm gas}+\rho_{\rm particle})}} \quad (15)$$

(Sekiya 1998; Cuzzi, Hogan & Shariff 2008; Shi & Chiang 2013). Equation (15) accounts for how particles not only add to the gravity of the clump (denominator), but also lower its effective sound speed from the pure-gas value $c_{\rm neb}$ (numerator), in the limit where the gas-particle mixture acts as a single fluid on the clump free-fall time; this limit is appropriate to chondrules which have short drag stopping times in the solar nebula. For parameters inspired by the simulation of Carter et al. (2019) ($\rho_{\rm gas} \sim 10^{-9}\,{\rm g\,cm^{-3}}$, $\rho_{\rm particle} \sim 10^{-6}\,{\rm g\,cm^{-3}}$, $c_{\rm neb} \sim 0.5\,{\rm km\,s^{-1}}$), we estimate $R_{\rm Jeans} \sim 4 \times 10^4$ km, which is ~40 times larger than the clump sizes reported by these authors, precluding gravitational instability. Turbulent motions only make it harder for particle overdensities to become bound (e.g. Klahr & Schreiber 2020a, b).

While gravitational instability in the immediate vicinity and aftermath of a vapourizing collision appears unviable, one could wait for chondrules to settle to the disc mid-plane, where they could concentrate and perhaps eventually self-gravitate. The streaming instability (Youdin & Goodman 2005) provides a route for particles to achieve super-Roche and super-Jeans densities (e.g. Carrera, Johansen & Davies 2015; Simon et al. 2017).

4 SUMMARY AND DISCUSSION

A theory for the formation of chondrules should explain how these mm-sized constituents of the oldest known asteroids were melted and cooled, and how they were collected with such efficiency as to fill $\gtrsim$50 per cent of the volume of meteorite parent bodies. In this paper, we have asked whether chondrites can form through hypervelocity (vapourizing) collisions between initially solid planetesimals, as suggested by many workers (e.g. Campbell et al. 2002; Krot et al. 2005; Fedkin et al. 2015; Johnson et al. 2015; 2016; Stewart et al. 2019b). We found that high-velocity collisions can reproduce the thermal histories of chondrules, but does not lend itself to understanding how they agglomerated into meteorite parent bodies.

In a hypervelocity collision between two asteroids, a fraction of the colliding mass is vapourized. We have detailed the thermal and dynamical evolution of the initially hot, overpressured vapour as it expands into the ambient nebula. The evolutionary stages of the vapour cloud include: (1) its initial free expansion and adiabatic cooling, (2) its condensation into dust grains which at first slow the cloud's cooling by releasing latent heat, and which later hasten cooling by radiating to space, (3) the cloud's deceleration due to loading by nebular gas, and (4) the cloud's eventual dissolution as nebular hydrogen backfills the near pressure-less cavity left by condensation. Against this evolving backdrop we have shown that solid/liquid particles entrained by the vapour cloud can experience heating and cooling episodes consistent with those inferred for chondrules: heating to the point of melting for a period of order 10^2 s, super-liquidus cooling at rates of 3000 K h^{-1} or more, and sub-liquidus cooling at rates of 3000 to $<$100 K h^{-1}.

Cooling rates vary primarily with the total mass of the vapour cloud. As cloud masses increase from 10^{17} to 10^{20} g, sub-liquidus cooling rates decrease from 1000 to 100 K h^{-1}. These cooling rates match those inferred experimentally for CB chondrules (Hewins et al. 2018). For these same cloud masses, plume temperatures and pressures vary from 2500 K and 10^{-2} bar on time-scales of minutes, to 1500 K and 10^{-6} bar over hours. These temperature and pressure ranges can reproduce the elemental abundances and zoning profiles of metal grains and chondrules in CB chondrites (Fedkin et al. 2015). Although this agreement is encouraging, we have not shown that our time-dependent plumes vary slowly enough to host the equilibrium condensation sequences that Fedkin et al. (2015) computed; moreover, their plume composition differs from ours, perhaps in significant ways.

With ab initio simulations of vapourizing collisions still under development (cf. Stewart et al. 2019b), it remains unclear how efficiently mass can be converted into vapour (see also Carter & Stewart 2020, who estimated the frequency of vapourizing collisions among planetesimals in the primordial asteroid belt, but did not quantify the amount of vapour produced). If we co-opt the jetted melt fractions computed by Johnson et al. (2015) and Wakita et al. (2017, 2021), and assume that roughly 1 per cent of the mass in colliding bodies is converted into vapour, then the cloud masses of 10^{17}–10^{20} g that we find reproduce CB chondrules implicate colliding planetesimals with radii of 10–100 km. Planetesimals in this size range are typical of the Solar system's minor body reservoirs (Morbidelli et al. 2009; Sheppard & Trujillo 2010). For conventional, non-CB chondrules whose porphyritic textures imply slower cooling

rates of 5–100 $K\,h^{-1}$ (Desch & Connolly 2002; Connolly & Jones 2016), our model scalings point to clouds having masses $\gtrsim 10^{22}$ g, or colliding bodies with radii $\gtrsim 500$ km. In some asteroid belt formation scenarios, many Ceres and Moon-sized bodies are thought to have populated the belt before being dynamically ejected (e.g. Wetherill 1992; Petit, Morbidelli & Chambers 2001; O'Brien, Morbidelli & Bottke 2007; Morbidelli et al. 2009).

If chondrules were ejected into the nebula by collisions, how did they agglomerate into a chondrite? High-velocity collisions are a double-edged sword: while they generate enough heat to melt chondrules, they also implicate a population of fast-moving planetesimals that cannot re-accrete chondrules efficiently and without damage. In the dynamically hot environment that we have envisioned, where non-circular velocities of large asteroids readily exceed $1\,km\,s^{-1}$ (corresponding to eccentricities and inclinations >0.05), gravitational focussing between chondrules and asteroids is negligible; an asteroid can accrete only those chondrules lying directly in its path, and not without shattering them on contact (Wurm et al. 2005; Teiser & Wurm 2009). Perhaps chondrules were accreted intact by especially small asteroids whose orbits were kept circular and co-planar by nebular gas drag. Other chondrule concentration mechanisms include the streaming instability (Youdin & Goodman 2005; Carrera et al. 2015; Simon et al. 2017), turbulent concentration (Hartlep & Cuzzi 2020), particle-aggregate sticking (Matsumoto et al. 2019), and trapping in overpressured, possibly self-gravitating gas rings (Tominaga, Takahashi & Inutsuka 2020). A stringent test of any agglomeration theory is presented by the CB/CH chondrite Isheyevo, whose sedimentary laminations imply gentle, layer-by-layer accretion of size and mineral-sorted material (Garvie et al. 2017). We have shown that the re-accretion/fallback scenario outlined by Morris et al. (2015) does not pass this test.

That accretion and shattering go hand-in-hand in high-velocity collision scenarios for chondrules might actually help to explain the 'chondrule fragments' collected from the coma of comet 81P/Wild-2 (e.g. Nakamura et al. 2008). These microchondrules may be the broken, micron-sized remains of mm-sized solids that fragmented upon being accreted on to comet progenitors/Kuiper belt objects. Chondrule fragments might similarly coat the surfaces of asteroids – they can be looked for in the *Hayabusa2* and *OSIRIS-REx* sample returns.

ACKNOWLEDGEMENTS

We thank Sarah Stewart for an inspiring talk that motivated this work, Steve Desch for an insightful referee report that led to qualitative changes to our paper, and Jeffrey Fung for prompting us to consider the effects of the nebular headwind and sharing his numerical simulations of solid/gas interactions. We thank Erik Asphaug, Bill Bottke, Don Brownlee, Linda Elkins-Tanton, Sivan Ginzburg, Brandon Johnson, Philipp Kempski, Sasha Krot, Rixin Li, Tomoki Nakamura, Laura Schaefer, Shigeru Wakita, Ben Weiss, and Andrew Youdin for useful exchanges. We are also grateful to the many people we talked with over the years about chondrules, including Jay Melosh. This work used the MATPLOTLIB (Hunter 2007) and SCIPY (Virtanen et al. 2020) packages, and was supported by National Aeronautics and Space Administration grant NNX15AD95G/NEXSS and Berkeley's Esper Larsen, Jr. fund.

DATA AVAILABILITY

No new data were generated or analysed in support of this research.

REFERENCES

Alexander C. M. O., Hutchison R., Barber D. J., 1989, Earth. Planet. Sc. Lett., 95, 187
Alexander C. M. O. D., Grossman J. N., Ebel D. S., Ciesla F. J., 2008, Science, 320, 1617
Armitage P. J., 2011, ARA&A, 49, 195
Asphaug E., Jutzi M., Movshovitz N., 2011, Earth. Planet. Sc. Lett., 308, 369
Bradley J. P., 1994, Geochim. Cosmochim. Acta, 58, 2123
Bridges J. C., Changela H. G., Nayakshin S., Starkey N. A., Franchi I. A., 2012, Earth. Planet. Sc. Lett., 341, 186
Brownlee D., Joswiak D., Matrajt G., 2012, Meteor. Planet. Sci., 47, 453
Brownlee D. E., Joswiak D. J., Bradley J. P., Matrajt G., Wooden D. H., 2005, in Mackwell S., Stansbery E., eds, 36th Annual Lunar and Planetary Science Conference. Lunar and Planetary Science Conference. p. 2391
Campbell A. J., Humayun M., Weisberg M. K., 2002, Geochim. Cosmochim. Acta, 66, 647
Carrera D., Johansen A., Davies M. B., 2015, A&A, 579, A43
Carter P. J., Stewart S. T., 2020, The Planetary Science Journal, 1, 45
Carter P. J., Davies E. J., Lock S. J., Stewart S. T., 2019, Lunar and Planetary Science Conference. Lunar and Planetary Science Conference. p. 1247
Chiang E., Youdin A. N., 2010, Annu. Rev. Earth. Pl. Sc., 38, 493
Connolly H. C., Jr, Jones R. H., 2016, J. Geophys. Res., 121, 1885
Cuzzi J. N., Hogan R. C., Shariff K., 2008, ApJ, 687, 1432
Davies E. J., Carter P. J., Root S., Kraus R. G., Spaulding D. K., Stewart S. T., Jacobsen S. B., 2020, J. Geophys. Res., 125, e06227
Dawson R. I., Murray-Clay R., 2012, ApJ, 750, 43
Desch S. J., Connolly H. C. J., 2002, Meteor. Planet. Sci., 37, 183
Dullemond C. P., Stammler S. M., Johansen A., 2014, ApJ, 794, 91
Dullemond C. P., Harsono D., Stammler S. M., Johansen A., 2016, ApJ, 832, 91
Ebel D. S., Grossman L., 2000, Geochim. Cosmochim. Acta, 64, 339
Fedkin A. V., Grossman L., 2013, Geochim. Cosmochim. Acta, 112, 226
Fedkin A. V., Grossman L., Humayun M., Simon S. B., Campbell A. J., 2015, Geochim. Cosmochim. Acta, 164, 236
Fegley Bruce J., Schaefer L., 2012, preprint (arXiv:1210.0270)
Fernandez J. A., Ip W. H., 1984, Icarus, 58, 109
Ford E. B., Chiang E. I., 2007, ApJ, 661, 602
Gainsforth Z. et al., 2015, Meteor. Planet. Sci., 50, 976
Gao P. et al., 2020, Nat. Astron., 4, 951
Garvie L. A. J., Knauth L. P., Morris M. A., 2017, Icarus, 292, 36
Gomes R., Levison H. F., Tsiganis K., Morbidelli A., 2005, Nature, 435, 466
Grossman L., Beckett J. R., Fedkin A. V., Simon S. B., Ciesla F. J., 2008, Rev. Mineral. Geochem., 68, 93
Hartlep T., Cuzzi J. N., 2020, ApJ, 892, 120
Hasegawa Y., Wakita S., Matsumoto Y., Oshino S., 2016a, ApJ, 816, 8
Hasegawa Y., Turner N. J., Masiero J., Wakita S., Matsumoto Y., Oshino S., 2016b, ApJ, 820, L12
Hewins R. H., Condie C., Morris M., Richardson M. L. A., Ouellette N., Metcalf M., 2018, ApJ, 855, L17
Hunter J. D., 2007, Comput. Sci. Eng., 9, 90
Ivanova M. A. et al., 2008, Meteor. Planet. Sci., 43, 915
Jacob D., Stodolna J., Leroux H., Langenhorst F., Houdellier F., 2009, Meteor. Planet. Sci., 44, 1475
Johansen A., Mac Low M.-M., Lacerda P., Bizzarro M., 2015, Sci. Adv., 1, 1500109
Johnson B. C., Melosh H. J., 2012, Icarus, 217, 416
Johnson B. C., Melosh H. J., 2014, Icarus, 228, 347
Johnson B. C., Minton D. A., Melosh H. J., Zuber M. T., 2015, Nature, 517, 339
Johnson B. C., Walsh K. J., Minton D. A., Krot A. N., Levison H. F., 2016, Sci. Adv., 2,e1601658
Klahr H., Schreiber A., 2020a, preprint (arXiv:2011.07849)
Klahr H., Schreiber A., 2020b, ApJ, 901, 54
Kraus R. G. et al., 2012, J. Geophys. Res., 117, E09009
Krot A., Ivanova M., Ulyanov A., 2007, Chemie der Erde / Geochem., 67, 283
Krot A. N., Amelin Y., Cassen P., Meibom A., 2005, Nature, 436, 989

Levison H. F., Morbidelli A., Tsiganis K., Nesvorný D., Gomes R., 2011, AJ, 142, 152
Lichtenberg T., Golabek G. J., Dullemond C. P., Schönbächler M., Gerya T. V., Meyer M. R., 2018, Icarus, 302, 27
Malhotra R., 1995, AJ, 110, 420
Matsumoto Y., Wakita S., Hasegawa Y., Oshino S., 2019, ApJ, 887, 248
Melosh H. J., 1989, Impact cratering
Melosh H. J., Vickery A. M., 1991, Nature, 350, 494
Messenger S., Keller L. P., Nguyen A. N., 2013, Proceedings of The Life Cycle of Dust in the Universe: Observations. p. 40
Morbidelli A., Bottke W. F., Nesvorný D., Levison H. F., 2009, Icarus, 204, 558
Morris M. A., Garvie L. A. J., Knauth L. P., 2015, ApJ, 801, L22
Nagahara H., Kushiro I., Mysen B. O., 1994, Geochim. Cosmochim. Acta, 58, 1951
Nakamura T. et al., 2008, Science, 321, 1664
Nelson V. E., Rubin A. E., 2002, Meteor. Planet. Sci., 37, 1361
Nesvorný D., Vokrouhlický D., Dones L., Levison H. F., Kaib N., Morbidelli A., 2017, ApJ, 845, 27
O'Brien D. P., Morbidelli A., Bottke W. F., 2007, Icarus, 191, 434
Ormel C. W., Klahr H. H., 2010, A&A, 520, A43
Petit J.-M., Morbidelli A., Chambers J., 2001, Icarus, 153, 338
Raymond S. N., Izidoro A., 2017, Icarus, 297, 134
Raymond S. N., Nesvorny D., 2020, preprint (arXiv:2012.07932)
Russell S., Connolly H., Krot A., 2018, Chondrules: Records of Protoplanetary Disk Processes. Cambridge Planetary Science. Cambridge Univ. Press, Cambridge
Sanders I. S., Scott E. R. D., 2012, Meteor. Planet. Sci., 47, 2170
Sekiya M., 1998, Icarus, 133, 298
Sheppard S. S., Trujillo C. A., 2010, ApJ, 723, L233
Shi J.-M., Chiang E., 2013, ApJ, 764, 20
Simon J. B., Armitage P. J., Youdin A. N., Li R., 2017, ApJ, 847, L12
Stewart S. T., Carter P. J., Davies E. J., Lock S. J., Kraus R. G., Root S., Petaev M. I., Jacobsen S. B., 2019a, Lunar and Planetary Science Conference. Lunar and Planetary Science Conference. p. 1250
Stewart S. T., Carter P. J., Davies E. J., Lock S. J., Kraus R. G., Root S., Petaev M. I., Jacobsen S. B., 2019b, Lunar and Planetary Science Conference. Lunar and Planetary Science Conference. p. 1251
Teiser J., Wurm G., 2009, MNRAS, 393, 1584
Tominaga R. T., Takahashi S. Z., Inutsuka S.-i., 2020, ApJ, 900, 182
Tsiganis K., Gomes R., Morbidelli A., Levison H. F., 2005, Nature, 435, 459
Virtanen P. et al., 2020, Nat. Methods, 17, 261
Wakita S., Matsumoto Y., Oshino S., Hasegawa Y., 2017, ApJ, 834, 125
Wakita S., Johnson B., Adeene Denton C., Davison T. M., 2021, Icarus, 360, 114365
Weidenschilling S. J., 1977, MNRAS, 180, 57
Weisberg M. K., McCoy T. J., Krot A. N., 2006, Systematics and Evaluation of Meteorite Classification, University of Arizona Press, Tucson, AZ, p. 19
Wetherill G. W., 1992, Icarus, 100, 307
Williams J. P., Cieza L. A., 2011, ARA&A, 49, 67
Wurm G., Paraskov G., Krauss O., 2005, Icarus, 178, 253
Youdin A. N., Goodman J., 2005, ApJ, 620, 459
Zel'dovich Y. B., Raizer Y. P., 1967, Physics of shock waves and high-temperature hydrodynamic phenomena, Dover Publications, US

This paper has been typeset from a TEX/LATEX file prepared by the author.